

Exact Coordinate Descent for High-Dimensional Regularized Huber Regression

Younghoon Kim*, Po-Ling Loh, Sumanta Basu

Abstract

We develop an exact coordinate descent algorithm for high-dimensional regularized Huber regression. In contrast to composite gradient descent methods, our algorithm fully exploits the advantages of coordinate descent when the underlying model is sparse. Moreover, unlike existing second-order approximation methods previously introduced in the literature, it remains effective even when the Hessian becomes ill-conditioned due to high correlations among covariates drawn from heavy-tailed distributions. The key idea is that, for each coordinate, marginal increments arise only from inlier observations, while the derivatives remain monotonically increasing over a grid constructed from the partial residuals. Building on conventional coordinate descent strategies, we further propose variable screening rules that selectively determine which variables to update at each iteration, thereby accelerating convergence. To the best of our knowledge, this is the first work to develop a first-order coordinate descent algorithm for penalized Huber loss minimization. We bound the nonasymptotic convergence rate of the proposed algorithm by extending arguments developed for the Lasso and formally characterize the operation of the proposed screening rule. Extensive simulation studies under heavy-tailed and highly-correlated predictors, together with a real data application, demonstrate both the practical efficiency of the method and the benefits of the computational enhancements.

Keywords: Coordinate descent, regularization path, robust regression, convex optimization, nonsmooth optimization, screening

1 Introduction

The field of robust statistics provides estimates that are resistant to outliers or extreme values [e.g., Hampel et al., 2011; Huber and Ronchetti, 2011; Maronna et al., 2019]. For location estimation, M-estimators generalize the mean by downweighting large deviations. In regression, this principle extends to coefficient estimation, producing models that capture the central trend of the response while reducing the influence of atypical observations. Robust regression thus naturally generalizes classical linear regression, maintaining the familiar linear framework, while offering greater stability in the presence of outliers.

Regularized Huber regression naturally bridges between classical linear regression and robust regression by incorporating both sparsity and robustness [e.g., Avella Medina and Ronchetti, 2015; Loh, 2024]. Specifically, for n pairs of $\{y_i, X_i\}_{i=1,\dots,n}$, where X_i is a p -dimensional vector of covariates and a response y_i , the coefficient vector $\hat{\beta}$ is estimated by minimizing a linear combination of a loss function and an ℓ_1 -penalty:

$$\hat{\beta} \in \arg \min_{\beta \in \mathbb{R}^p} \left\{ F(\beta) := f(\beta) + \lambda \|\beta\|_1 := \frac{1}{n} \sum_{i=1}^n w_i \rho_\delta(y_i - X_i^\top \beta) + \lambda \|\beta\|_1 \right\}, \quad (1)$$

*Corresponding author. Email: yk748@cornell.edu

where $\rho_\delta(u)$ is the Huber loss with threshold δ , which behaves quadratically for small residuals and linearly for large residuals:

$$\rho_\delta(u) = \begin{cases} \frac{1}{2}u^2, & \text{if } |u| \leq \delta, \\ \delta|u| - \frac{1}{2}\delta^2, & \text{if } |u| > \delta, \end{cases} \quad (2)$$

and has derivative

$$\rho'_\delta(u) = \begin{cases} u, & \text{if } |u| \leq \delta, \\ \delta\text{sign}(u), & \text{if } |u| > \delta. \end{cases} \quad (3)$$

The weights $\{w_i\}_{i=1,\dots,n}$ provide further flexibility in estimation. Note that the precise form of the robust regression objective in (1) may vary slightly across different contexts [see Section 2.2. in Loh, 2021]. For simplicity, we consider $\{w_i = 1\}_{i=1,\dots,n}$ throughout the study. In the context of regularized robust regression, the most basic form of Huber regression considered in this work highlights the connection between classical linear regression (quadratic loss) and robust regression (Huber loss), while incorporating sparsity through the ℓ_1 -penalty.

For high-dimensional regression models, incorporating sparsity into estimation enhances interpretability and might be expected to lend computational efficiency. However, in the context of regularized robust regression, most existing algorithms rely on full-gradient methods and do not fully exploit sparsity [e.g., Nesterov, 2013b; Sun et al., 2016; Beck, 2017]. In particular, such a full-gradient approach is prevalent in robust regression. As a result, previous methods require computing the full gradient at each iteration, which can be computationally expensive and limit scalability in high-dimensional settings.

Coordinate descent algorithms offer outstanding performance for high-dimensional regression with sparsity [e.g., Wright, 2015; Shi et al., 2016]. Despite their potential, however, few studies have explored their application in regularized robust regression, leaving opportunities for further research and algorithmic development. Evaluating robust regression methods also requires accounting for extreme data conditions, such as highly-correlated covariates and heavy-tailed distributions. A coordinate descent algorithm specifically designed to perform reliably under these challenging settings has thus been lacking.

1.1 Related Work

In this section, we introduce several existing benchmarks that can be used to optimize the penalized Huber regression objective. First, as the most common approach, composite gradient descent [CGD or simply GD; e.g., Nesterov, 2013a] can be employed. Indeed, this method has been featured in simulation studies in theoretical work on robust statistics [e.g., Loh, 2017, 2021]. On the k^{th} iteration, the algorithm computes

$$\begin{aligned} \beta^{k+1} &\in \arg \min_{\beta} \left\{ f(\beta^{(k)}) + \langle \nabla f(\beta^{(k)}), \beta - \beta^{(k)} \rangle + \frac{\eta}{2} \|\beta - \beta^{(k)}\|_2^2 + \lambda \|\beta\|_1 \right\} \\ &= \arg \min_{\beta} \left\{ \frac{1}{2} \left\| \beta - \left(\beta - \frac{1}{\eta} \nabla f(\beta^{(k)}) \right) \right\|_2^2 + \frac{\lambda}{\eta} \|\beta\|_1 \right\} \\ &= S_{\lambda/\eta} \left(\beta^{(k)} - \frac{1}{\eta} \nabla f(\beta^{(k)}) \right), \end{aligned} \quad (4)$$

where η is the stepsize and S_τ is the soft-thresholding shrinkage operator,

$$(S_\tau(v))_i = \text{sign}(v_i) \cdot \max(|v_i| - \tau, 0). \quad (5)$$

Conventionally, one takes $\eta = 1/L$ with $L = \frac{1}{n} \text{eig}_{\max}(X^\top X)$, where X is $n \times p$ -dimensional covariates and $\text{eig}_{\max}(M)$ is the largest eigenvalue of the matrix M .

Recently, Sun et al. [2020] applied the iterative local adaptive majorize-minimization method [I-LAMM; Fan et al., 2018], a computational framework built on the majorization-minimization (MM) algorithm [see Sun et al., 2016, for a comprehensive survey]. The idea is as follows: at the k^{th} iteration, one constructs

a so-called majorizing function $h(\beta|\beta^{(k)})$ for the given function $f(\beta)$ with respect to β , given the current iterate $\beta^{(k)}$, such that it satisfies

$$h(\beta|\beta^{(k)}) \geq f(\beta), \quad h(\beta^{(k)}|\beta^{(k)}) = f(\beta^{(k)}). \quad (6)$$

If the properties in (6) are satisfied, the value of the objective function decreases in each iteration, since

$$f(\beta^{(k+1)}) \leq h(\beta^{(k+1)}|\beta^{(k)}) \leq h(\beta^{(k)}|\beta^{(k)}) = f(\beta^{(k)}).$$

Thus, we majorize $f(\beta)$ at $\beta^{(k)}$ by

$$h_k(\beta|\beta^{(k)}) = f(\beta^{(k)}) + \langle \nabla f(\beta^{(k)}), \beta - \beta^{(k)} \rangle + \frac{\eta_k}{2} \|\beta - \beta^{(k)}\|_2^2,$$

where η_k is a parameter such that $h_k(\beta^{(k+1)}|\beta^{(k)}) \geq f(\beta^{(k+1)})$, which can be tuned at each iteration. Hence, the algorithm solves

$$\begin{aligned} \beta^{(k+1)} &\in \arg \min_{\beta} \left\{ \langle \nabla f(\beta^{(k)}), \beta - \beta^{(k)} \rangle + \frac{\eta_k}{2} \|\beta - \beta^{(k)}\|_2^2 + \lambda \|\beta\|_1 \right\} \\ &= S_{\lambda/\eta_k} \left(\beta^{(k)} - \frac{1}{\eta_k} \nabla f(\beta^{(k)}) \right), \end{aligned}$$

where S_τ is defined in (5).

So far, the two methods discussed above are full-gradient approaches, where the ℓ_1 -penalty is applied only at the final step to shrink small-scale estimates. An alternative is the coordinate descent algorithm recently proposed by Yi and Huang [2017], which leverages a second-order (Newton) local approximation [e.g., Mifflin, 1977; Chen, 2012] for nonsmooth functions, applicable to the Huber loss. Note the Karush–Kuhn–Tucker (KKT) condition of (1):

$$-\frac{1}{n} \sum_i \rho_\delta^\top (y_i - X_i^\top \beta) X_{ij} + \lambda s_j = 0, \quad (7)$$

$$\beta_j - S_1(\beta_j + s_j) = 0, \quad (8)$$

where S_1 is again in (5) with $\tau = 1$. We illustrate how the update for each coordinate is performed at a fixed k^{th} iteration. To simplify the notation, we omit the index k . Take $\tilde{r}_i = y_i - x_j^\top \tilde{\beta}$, where $\tilde{\beta}_j$ and \tilde{s}_j are variables such that at each step, the values of the other variables $j' \neq j$ are fixed. From (7) and (8), we have

$$h_j(\tilde{\beta}, z) = \begin{bmatrix} -\frac{1}{n} \sum_i \rho_\delta(\tilde{r}_i + X_{ij} \tilde{\beta}_j - X_{ij} z_1) X_{ij} + \lambda z_2, \\ z_1 - S_\lambda(z_1 + z_2) \end{bmatrix},$$

where the second element is

$$z_1 - S_\lambda(z_1 + z_2) = \begin{cases} -z_2 + \text{sign}(z_1 + z_2), & \text{if } |z_1 + z_2| > 1, \\ z_1, & \text{if } |z_1 + z_2| \leq 1. \end{cases}$$

Note that the range of $z_1 + z_2$ determines the update at each coordinate. Hence, the update is obtained by linearizing the Huber loss using their generalized derivatives [e.g., Clarke, 1990]:

$$\begin{bmatrix} \beta_j \\ s_j \end{bmatrix} \leftarrow \begin{bmatrix} \tilde{\beta}_j \\ \tilde{s}_j \end{bmatrix} - H_j(\tilde{\beta}_j, \tilde{s}_j)^{-1} h_j(\tilde{\beta}_j, \tilde{s}_j) = \begin{cases} \begin{bmatrix} \tilde{\beta}_j + \frac{\frac{1}{n} \sum_i \rho'_\delta(\tilde{r}_i) X_{ij} - \lambda \text{sign}(\tilde{\beta}_j + \tilde{s}_j)}{\frac{1}{n} \sum_i \psi_\delta(\tilde{r}_i) X_{ij}^2} \\ \text{sign}(\tilde{\beta}_j + \tilde{s}_j) \end{bmatrix}, & |\tilde{\beta}_j + \tilde{s}_j| > 1, \\ \begin{bmatrix} 0 \\ \frac{\frac{1}{n} \sum_i \rho'_\delta(\tilde{r}_i) X_{ij} + \tilde{\beta}_j \frac{1}{n} \sum_i \psi_\delta(\tilde{r}_i) X_{ij}^2}{\lambda} \end{bmatrix}, & |\tilde{\beta}_j + \tilde{s}_j| \leq 1, \end{cases}$$

where $\psi_\delta(u) = 1_{\{|u| \leq \delta\}}$ and

$$H_j(\tilde{\beta}, z) = \begin{bmatrix} \frac{1}{n} \sum_i \psi_\delta(\tilde{r}_i + X_{ij} \tilde{\beta}_j - X_{ij} z_1) X_{ij}^2 & \lambda \\ 1_{\{|z_1 + z_2| \leq 1\}} & -1_{\{|z_1 + z_2| > 1\}} \end{bmatrix}.$$

1.2 Contributions

In this paper, we introduce a pathwise coordinate descent algorithm (hereafter referred to simply as *coordinate descent*) for estimating parameters in ℓ_1 -regularized Huber regression. The method is inspired by the coordinate descent approach for penalized regression [Friedman et al., 2007].

We establish convergence guarantees and present practical computational strategies to accelerate the algorithm. To the best of our knowledge, this is the first work to develop a first-order coordinate descent method for composite function minimization in which both the loss and penalty terms are nonsmooth. In particular, compared to the benchmark methods that rely on second-order approximations, our proposed method remains effective under ill-conditioned design matrices, such as those with correlated columns or heavy-tailed distributions. We illustrate the performance of our algorithm through numerical experiments that specifically consider these challenging scenarios.

Finally, we provide an R package, `rome`, designed in a similar manner as the well-known `glmnet` [Friedman et al., 2010], making it easy for potential users to become familiar with our package.

1.3 Organization of the Paper

The rest of this paper is organized as follows: Section 2 introduces the essential ideas, motivated by the example of calculating a univariate Huber location estimator and extending it to penalized Huber regression. Section 3 presents computational techniques that accelerate convergence of the algorithm and establishes theoretical guarantees for both the algorithm and the suggested techniques. Section 4 reports numerical experiments, including comparisons with benchmark methods, demonstrations of the effectiveness of the computational accelerations, and a data application. Section 5 concludes with a discussion.

2 Proposed Method

2.1 Huberized Median for Univariate Samples

We explain the proposed algorithm by illustrating the univariate Huberized median problem, possibly with a penalty term. Suppose we have n observations $\{X_1, \dots, X_n\}$ and $\lambda \geq 0$. Then the Huberized median is obtained by solving

$$\hat{c} \in \arg \min_{c \in \mathbb{R}} \left\{ f(c) = \sum_{i=1}^n \rho_\delta(X_i - c) + \lambda|c| \right\}. \quad (9)$$

Recall the Huber loss (2) with threshold $\delta > 0$, which can be written as

$$\rho_\delta(u) = \frac{u^2}{2} \mathbf{1}_{\{|u| \leq \delta\}} + \left(\delta|u| - \frac{\delta^2}{2} \right) \mathbf{1}_{\{|u| > \delta\}}.$$

Its derivative (3) is then

$$\rho'_\delta(u) = u \mathbf{1}_{\{|u| < \delta\}} + \delta \text{sign}(u) \mathbf{1}_{\{|u| > \delta\}}.$$

Using this expression, the derivative of $f(c)$ in (9) with respect to c is

$$f'(c) = \sum_{i; |X_i - c| \leq \delta} (c - X_i) + \delta \sum_{i; |X_i - c| > \delta} \text{sign}(c - X_i) + \lambda \text{sign}(c). \quad (10)$$

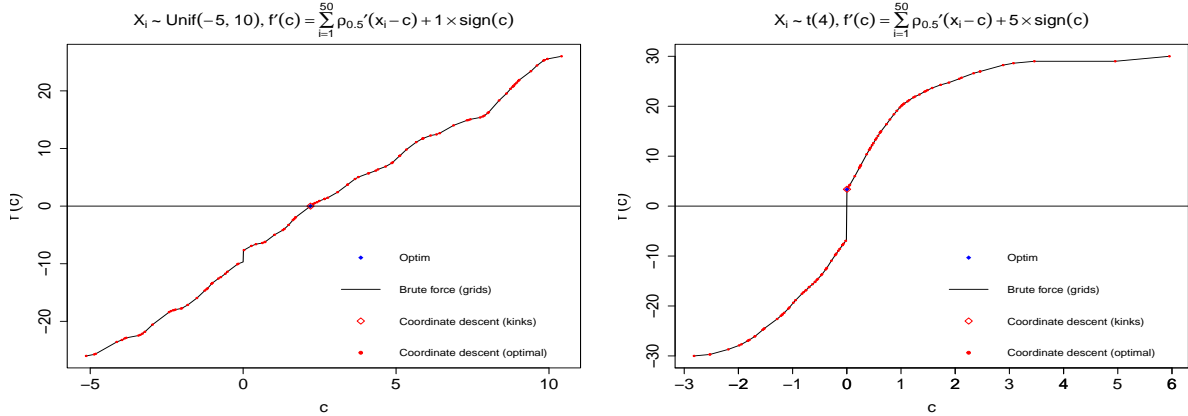


Figure 1: Illustration of the Huberized medians for Data I (left) and Data II (right) under different values of λ . The plots display the solutions obtained by the coordinate descent algorithm (red diamond), the ordered kinks used for the algorithm (red dots), the results of a grid search evaluating $f'(c)$ over a range of c values (black line), and the solution from a univariate optimization solver applied to $f(c)$ (blue diamond).

We wish to find c such that $f'(c) = 0$ in (10). Among the two summations in (10), the i^{th} observation belongs to exactly one, determined by the location of c . Specifically, the marginal contribution of the i^{th} observation to the derivative is

$$S_i = \begin{cases} -\delta, & \text{if } c < X_i - \delta, \\ 1 \times (c - (X_i - \delta)) - \delta, & \text{if } X_i - \delta < c < X_i + \delta, \\ \delta, & \text{if } c > X_i + \delta. \end{cases} \quad (11)$$

Hence, the marginal increment S_i remains $-\delta$ when $c < X_i - \delta$, increases linearly with slope 1 over the interval $(X_i - \delta, X_i + \delta)$, and reaches δ once $c > X_i + \delta$.

The structure of the marginal contribution in (11) implies that as c varies, the incremental change can be determined simply by counting how many observations have c within their intervals $(X_i - \delta, X_i + \delta)$. The increment is then proportional to the number of such observations relative to the total. A straightforward way to locate the potential value of c is to use a grid search: construct a fine grid from $\min_i(X_i - \delta)$ to $\max_i(X_i + \delta)$, and trace the trajectory of $f'(c)$ to identify where it crosses zero. Obviously, this trajectory is monotonically increasing.

Suppose we construct a grid of $2n$ points from the observations and the thresholds, $\{X_1 - \delta, X_1 + \delta, \dots, X_n - \delta, X_n + \delta\}$. Sorting these values yields the ordered sequence $v_1 \leq v_2 \leq \dots \leq v_{2n}$, called *kinks*. We then compute the cumulative sum of the slopes of the marginal contributions (11). Note that the increment for each observation is proportional to the length taken in the interval $(X_i - \delta, X_i + \delta)$. In this setting, it suffices to check whether the current kink v_m , for $m = 1, \dots, 2n$, is contained within an interval, since the order of the left and right endpoints remains unchanged after sorting. The optimal solution \hat{c} thus lies between two consecutive kinks, v_m and v_{m+1} , such that $f'(v_m) < 0$ and $f'(v_{m+1}) > 0$. We again use the fact that this trajectory is monotonically increasing.

In addition, the penalty parameter λ introduces a $\pm\lambda$ adjustment around zero for c , encouraging the optimal solution \hat{c} to shrink toward zero. This effect is analogous to the soft-thresholding operator induced by the ℓ_1 -penalty.

2.1.1 Two Examples

To visualize the algorithm, we present two examples that illustrate quite different cases. In the first example, suppose we draw 50 random samples from a uniform distribution on $[-5, 10]$. In this case, the Huberized median is unlikely to lie at zero. The left panel of Figure 1 shows the grid search results (black lines) with the kinks marked in red, all of which lie exactly on the constructed grid. Since the Huberized median is located away from zero, the zero-crossing of $f'(c)$ also occurs away from zero. Thus, introducing a penalty term with $\lambda = 1$ does not boost the location of the optimal solution close to zero.

In the second example, we consider 50 random samples from a t -distribution with 4 degrees of freedom. Aside from a few outliers, most observations are symmetrically distributed, so the Huberized median is likely to fall near zero. The right panel of Figure 1 displays the results using the same representation as in the first example, with all kinks again lying exactly on the constructed grid. Unlike the previous case, however, since the median is close to zero, adding the penalty term with $\lambda = 5$ shifts the solution so that the zero-crossing occurs at zero.

2.2 Extension to Penalized Huber Regression

We extend the idea of the Huberized median introduced in Section 2.1 to derive the estimator for penalized Huber regression. While the `rome` package can also accommodate weighted versions of (1), similar to adaptive Huber regression [e.g., Loh, 2021], the approach throughout this study focuses on the unweighted case. Accordingly, we assume $w_i = 1$ for all $i = 1, \dots, n$. In this section, we also omit the index k for iterations.

Recall the regularized Huber regression objective in (1):

$$\hat{\beta} \in \arg \min_{\beta \in \mathbb{R}^p} \left\{ f(\beta) := \frac{1}{n} \sum_{i=1}^n \rho_\delta(y_i - X_i^\top \beta) + \lambda \|\beta\|_1 \right\}. \quad (12)$$

For each $j = 1, \dots, p$ variable, the coordinate descent algorithm solves

$$\hat{\beta}_j \in \arg \min_{\beta_j \in \mathbb{R}} \left\{ f(\beta_j) =: \frac{1}{n} \sum_{i=1}^n \rho_\delta(X_{ij}(r_{ij} - \beta_j)) + \lambda |\beta_j| \right\}, \quad (13)$$

where $r_{ij} = r_{ij}(\beta_j) = \frac{y_i - \sum_{k \neq j} X_{ij} \hat{\beta}_k}{X_{ij}}$ is the partial residual of the j^{th} variable, for $i = 1, \dots, n$. Similar to (10), the derivative of the penalized regression with respect to the j^{th} variable is

$$f'(\beta_j) = \frac{1}{n} \sum_{i:|r_{ij}-\beta_j| \leq \delta/|X_{ij}|} X_{ij}^2(\beta_j - r_{ij}) + \frac{\delta}{n} \sum_{i:|r_{ij}-\beta_j| > \delta/|X_{ij}|} |X_{ij}| \text{sign}(\beta_j - r_{ij}) + \lambda \text{sign}(\beta_j).$$

Now, the term r_{ij} at the j^{th} variable plays the role of observations at the univariate Huberized median. The marginal contribution of the i^{th} observation to $f'(\beta_j)$ is

$$S_i(r_{ij}(\beta_j)) = \begin{cases} -\frac{|X_{ij}|}{n}, & \text{if } \beta_j < r_{ij} - \delta/|X_{ij}|, \\ \frac{X_{ij}^2}{n} \times (\beta_j - (r_{ij} - \delta/|X_{ij}|)) - \frac{|X_{ij}|}{n}, & \text{if } r_{ij} - \delta/|X_{ij}| < \beta_j < r_{ij} + \delta/|X_{ij}|, \\ \frac{|X_{ij}|}{n}, & \text{if } \beta_j > r_{ij} + \delta/|X_{ij}|. \end{cases} \quad (14)$$

Analogous to the case of the Huberized median, we obtain $2n$ kinks by sorting the set $\{r_{1j} - \delta/|X_{1j}|, r_{1j} + \delta/|X_{1j}|, \dots, r_{nj} - \delta/|X_{nj}|, r_{nj} + \delta/|X_{nj}|\}$ in increasing order. The cumulative slope at each kink v_m is then computed as

$$\sum_{i:v_m \in [r_{ij} - \delta/|X_{ij}|, r_{ij} + \delta/|X_{ij}|]} \frac{X_{ij}^2}{n},$$

for $m = 1, \dots, 2n$, where the summation accounts for all i such that v_m falls within the corresponding interval. The algorithm repeats this operation for each coordinate across iterations $k = 1, 2, \dots$ until convergence.

The remaining steps of the algorithm follow those of `glmnet` [Friedman et al., 2010], in the sense that we employ pathwise updates along a decreasing sequence of regularization parameters, use warm starts to accelerate convergence, and apply a screening rule to restrict updates to variables that are likely to be nonzero [see also Chapter 5.4 in Hastie et al., 2015].

Remark 2.1. To the best of our knowledge, there is no practical, universal rule to obtain the optimal weights $\{w_i\}_{i=1,\dots,n}$ and threshold δ . In terms of the weights, we adopt Mallows-type reweighting to improve robustness against high-leverage points by modifying the Huber loss with covariate-dependent weights. Specifically, in the adaptive penalized Huber regression (1), we set $w_i = w(X_i) = \min\{1, b/\|X_i\|_2\}$ for some constant b . In this way, $w(X_i)$ adjusts according to the leverage of the i^{th} observation, measured by $\|X_i\|_2$, thereby reducing the influence of covariates with unusually large norms [see also Section 3.2 in Loh, 2017]. From an algorithmic perspective, this is equivalent to replacing (y_i, X_{ij}) with $(w_i y_i, w_i X_{ij})$, so the computational procedure remains unchanged.

The choice of the threshold parameter δ is more complicated due to its relationship to the scale of the additive errors, usually assumed to be unknown a priori [e.g., Chapter 7.7 in Huber and Ronchetti, 2011]. Combining our approach with methods such as optimizing Huber's concomitant estimator to obtain the scale parameter is beyond the scope of our current analysis, and is left for future research [see Section 3 in Loh, 2021, for a related discussion].

2.3 Theory of Convergence

This section presents a convergence guarantee for the algorithm proposed in Section 2.2.

Proposition 2.1 (Convergence of the algorithm). *Let $\beta^{(k)}$ denote the solution at the k^{th} iteration. For any minimizer β^* of $F(\beta)$ in (1) and for all $k \geq 1$, we have*

$$F(\beta^{(k)}) - F(\beta^*) \leq \frac{L_H \|\beta^{(0)} - \beta^*\|_2^2}{k}, \quad (15)$$

where the Lipschitz constant L_H of the Huber loss is bounded by $L_H \leq \frac{1}{n} \text{eig}_{\max}(X^T X)$. Hence, the optimality gap $F(\beta^{(k)}) - F(\beta^*)$ converges to 0 as $k \rightarrow \infty$.

It is not surprising that the speed of convergence $O(1/k)$ commonly appears in gradient descent-type (first-order) methods [e.g., Nesterov, 2013b; Beck, 2017]. However, it can be shown that the convergence rate of the coordinate descent algorithm is *faster* than that of the gradient descent algorithm, as explained in Section 1.1.

We follow the proof strategy of Saha and Tewari [2013]. Here, two assumptions are required: (i) for a p -dimensional ($p \geq 1$) variable α , the operator $\alpha \mapsto \alpha - \frac{\nabla f(\alpha)}{L}$ is monotonically increasing, and (ii) for any $j = 1, \dots, p$, the univariate function corresponding to the j^{th} variable at the k^{th} iteration is strictly convex. The proof of Proposition 2.1 and the necessary details from Saha and Tewari [2013] required to complete the argument are provided in Appendix B.

Note that the first assumption (i) holds whenever the Lasso (ℓ_1 -penalty term) is used. On the other hand, the second assumption (ii) needs to be relaxed. Specifically, this assumption serves to bound τ_j , the coordinate slope in terms of the j^{th} variable, defined as

$$\tau_j = \frac{g'_j(z_j^{(k,j)}) - g'_j(z_j^{(k,j-1)})}{z_j^{(k,j)} - z_j^{(k,j-1)}}, \quad (16)$$

where $g_j(\alpha_j) = F_j(\alpha_j; z_j^{(k,j-1)})$, $z_j^{(k,j)}$ is the solution of the j^{th} variable updated at the k^{th} iteration, and $z_j^{(k,j-1)}$ is the solution of the j^{th} variable before the nontrivial update for that coordinate in the same iteration (i.e., within the same k^{th} iteration, the updates have been from the 1st to $(j-1)^{\text{th}}$ variables). Here, the challenge lies in determining the range of τ_j , particularly its upper bound L_H , which depends on the coordinate j , unlike in the case of the squared ℓ_2 -loss. Conceptually, however, the secant (16) remains tight with respect to the true derivative (see Figure 1 for an illustration).

3 Computational Advancements

In this section, we present several computational strategies designed to improve the rate of convergence of our algorithm. We also establish theoretical guarantees to ensure the convergence of the proposed method. Throughout these sections, we omit the index k for iterations.

3.1 Warm Starts

In practice, it is common to compute a sequence of Lasso solutions over a decreasing grid of regularization parameters $\{\lambda_\ell\}_{\ell=1,\dots,\ell_{\max}}$. In **rome**, we use $\ell_{\max} = 100$ as a default. The maximum value of the λ sequence is

$$\lambda_{\max} = \lambda_1 = \frac{1}{n} \left| \max_j \sum_{i=1}^n X_{ij} \rho'_\delta(y_i) \right|,$$

where $\rho'_\delta(u)$ is the derivative of the Huber loss function (3). This choice is consistent with the convention of selecting the largest value using the null deviance in the Lasso. Following the approach of the **glmnet** package, the grid is constructed by decreasing λ from λ_1 down to $\lambda_L = \epsilon \lambda_1$ on a log scale. The default in **rome** is set as $\epsilon = 0.05$. Each solution $\hat{\beta}(\lambda_\ell)$ then serves as an effective warm start for obtaining $\hat{\beta}(\lambda_{\ell+1})$. Similarly, the number of nonzero coefficients tends to increase gradually with ℓ .

3.2 Adaptive Sequential Strong Rules

Along with the warm start described in Section 3.1, another widely used computational strategy in coordinate descent algorithms is the sequential strong (screening) rule, which identifies a subset of variables likely to be active. The most prominent example is the sequential strong rule [Tibshirani et al., 2012]. However, as noted by Yi and Huang [2017], the conventional setting used in Lasso programs is often unsuitable, as violations are frequently observed. To address this, they proposed a variant known as the adaptive sequential strong rule.

Recall the KKT conditions (7) and (8). Define $c_j(\lambda) = -\frac{1}{n} \sum_i \rho'_\delta(y_i - X_i^\top \hat{\beta}) X_{ij}$. Then one has

$$|c_j(\lambda)| \leq \lambda - \frac{\|X_i\|_2 \|y\|_2}{\lambda_{\max}} (\lambda_{\max} - \lambda) = \lambda - \frac{\|X_i\|_2 \|y\|_2}{\max_i |X_i^\top \rho_\delta(y_i)|} (\lambda_{\max} - \lambda) := \lambda + M(\lambda - \lambda_{\max}).$$

In order for each c_j to be Lipschitz continuous, we need

$$|c_j(\lambda) - c_j(\lambda')| \leq M(\lambda - \lambda').$$

The sequential strong rule of Tibshirani et al. [2012] is obtained by replacing λ with λ_ℓ , and λ_{\max} and λ' with $\lambda_{\ell-1}$, respectively, and setting $M = 1$ for all ℓ . The adaptive sequential strong rule of Yi and Huang [2017] allows M to vary with λ_ℓ , say M_ℓ . In our algorithm, we adopt the latter version without further

modification. However, note that the KKT condition in Step 2 below is described in Section 3.3, and it differs from the one given therein.

In summary, for a sequence of $\lambda_1 \geq \lambda_2 \geq \dots \geq \lambda_{\ell_{\max}}$:

- Derive the eligible set of predictors as $\mathcal{E} = \{j : |c_j(\lambda_{\ell-1})| \geq \lambda_\ell + M_{\ell-1}(\lambda_\ell - \lambda_{\ell-1})\}$, where $M_0 = 1$ and

$$M_\ell = \frac{\max_j |c_j(\lambda_{\ell-1}) - c_j(\lambda_\ell)|}{\lambda_{\ell-1} - \lambda_\ell}. \quad (17)$$

- Solve the problem (13) using only the predictors $j \in \mathcal{E}$. Check the KKT conditions for $j \notin \mathcal{E}$, and include any j that violates the KKT conditions back into \mathcal{E} .
- Compute M_ℓ .

We conduct a numerical experiment comparing the two rules: the strong screening rule and its adaptive version described in this section. The results are presented in Section 4.2.

3.3 Checking Optimality Conditions

A novel computational strategy applicable to our algorithm is the use of KKT condition (optimality condition) checks. In `rome`, these checks are performed only for variables outside the set \mathcal{E} at step 2 of the adaptive sequential strong rule in Section 3.2. But in principle, they can be applied independently of the screen rule. In other words, if the strong rule is not applied, one can simply set $\mathcal{E} = \emptyset$ so that $\mathcal{E}^c = \{1, 2, \dots, p\}$. In this case, the algorithm updates all variables at every iteration.

In the algorithm described in Section 2, Quicksort is used for reordering kinks. Quicksort is a widely used sorting algorithm that follows a divide-and-conquer strategy: it selects a pivot, partitions the array into elements less than and greater than the pivot, and recursively sorts the subarrays. On average, the quicksort algorithm reorders n elements in $O(n \log n)$ arithmetic operations, which results from performing $O(n)$ work per partition step across $\log n$ levels of recursion. In the worst case, when the pivot choices lead to highly unbalanced partitions, the complexity can degrade to $O(n^2)$ [e.g., see Chapter 7 in Cormen et al., 2022]. However, this scenario is unlikely in our context, since the order of half of the $2n$ kink points is predetermined.

In the context of the penalized Huber regression algorithm, the arithmetic cost per coordinate update is dominated by sorting the $2n$ kink points generated from the partial residuals $\{r_{ij}\}_{i=1, \dots, n}$ for each j^{th} variable. The remaining computations, such as computing cumulative slopes, locating the root where the derivative crosses zero, and updating the global residual vector, require only linear $O(n)$ operations. Consequently, each coordinate update has complexity $O(n \log n)$, and a full sweep across all variables requires $O(pn \log n)$ arithmetic operations. This is unusual for coordinate descent algorithms, as the computational cost typically scales with the number of variables p , not with the number of samples n [e.g., Richtárik and Takáč, 2014]. Therefore, it is necessary to develop strategies that reduce the number of variables updated in each iteration.

This idea is inspired by Kim and Basu [2025] (see Proposition 3.1 therein). In quantile regression, the condition relies only on the signs of X_{ij} in the design matrix: once a sign changes, it remains constant thereafter. By contrast, in Huber regression, one must verify whether each observation's marginal contribution is increasing; that is, whether the candidate solution lies within the interval defined by the partial residuals and the threshold. Consequently, the condition to be checked is more complex, but the following results show that a similar argument holds in a more general sense.

Proposition 3.1 (Karush-Kuhn-Tucker (KKT) condition). *For each j^{th} variable, the following conditions characterize the update:*

(a) Define $c_j(\beta_j)$ as the value of (13) with β_j . If $\mathcal{I}(\beta_j)$ is the set of indices $i = 1, \dots, n$ that satisfy $|\beta_j - r_{ij}| \leq \delta/|x_{ij}|$, then

$$c_j(\beta_j) = S_0 + \frac{1}{n} \sum_{i \in \mathcal{I}(\beta_j)} (X_{ij}^2(\beta_j - r_{ij}) + \delta|x_{ij}|) + \lambda \operatorname{sign}(\beta_j), \quad (18)$$

where $S_0 = -\frac{\delta}{n} \sum_{i=1}^n |x_{ij}|$.

(b) Assume that the kinks $\{v_m\}$ are distinct. The nontrivial solution β_j is obtained when $c_j(\beta_j; \mathcal{I})c_j(\beta_j; \mathcal{I}') < 0$ for index sets $\mathcal{I}, \mathcal{I}'$ such that $\mathcal{I} \subset \mathcal{I}'$ and $|\mathcal{I}' \setminus \mathcal{I}| = 1$.

(c) The minimizer $\hat{\beta}_j$ of (13) is zero if and only if the KKT condition,

$$|c_j(0)| \leq \lambda, \quad (19)$$

holds.

This step is performed prior to each coordinate update. The computed partial residuals used in checking the KKT condition (19) are then re-utilized in the update, if necessary.

Proof. The statement (a) is immediate. For (b), take $\lambda = 0$ first. Note that between any two consecutive kink points $v_m = r_{ij} - \delta/|X_{ij}|$ and $v_{m+1} = r_{ij} + \delta/|X_{ij}|$, the set $\mathcal{I}(\beta_j)$ remains constant, and so do the values of $c_j(\beta_j)$ at the kinks. On the interval constructed by those two kinks, the function $c'_j(\beta_j)$ in (18) is affine:

$$c'_j(\beta_j) = \frac{1}{n} \sum_{i \in \mathcal{I}'(\beta_j)} X_{ij}^2 \geq 0,$$

which implies that the derivative is monotonically increasing. Let two consecutive kink points be $v_m < v_{m+1}$. Let the sets $\mathcal{I}, \mathcal{I}'$ be the outside set on (v_m, v'_{m+1}) to the left and right of the kink that they share. This implies $\mathcal{I} \subset \mathcal{I}'$ and $|\mathcal{I}' \setminus \mathcal{I}| = 1$. On (v_m, v_{m+1}) , note that \mathcal{I} is fixed and $c'_j(\beta_j)$ is affine with nonnegative slope. Consider the two affine functions $c'_j(\beta_j; \mathcal{I})$ and $c'_j(\beta_j; \mathcal{I}')$. By the Intermediate Value Theorem, $c_j(\beta_j; \mathcal{I})c_j(\beta_j; \mathcal{I}') < 0$ implies that there exists $\tilde{\beta}_j \in (v_m, v_{m+1})$ such that $c_j(\tilde{\beta}_j) = 0$. Since $c'_j(\beta_j)$ is nonnegative, the $\tilde{\beta}_j$ is unique in (v_m, v_{m+1}) . For the case $\lambda > 0$, the KKT condition becomes

$$c'_j(\beta_j) + \lambda \operatorname{sign}(\beta_j) = 0,$$

meaning that $c'_j(\beta_j)$ is still affine with $\pm\lambda$ shifts. Therefore, a nonzero solution lies in an interval bounded by two consecutive kinks exactly when the two affine functions take opposite signs at their right and left boundaries. For (c), at $\beta_j = 0$, the KKT condition becomes

$$0 \in c'_j(0) + \lambda z, \quad z \in [-1, 1],$$

which is equivalent to (19). □

To support the usefulness of checking the optimality condition (19) before updating variables, we report results comparing computation times with and without checking this condition as another part of the numerical experiments. The results are presented in Section 4.2.

4 Numerical Illustrations

4.1 First Numerical Study

We conduct numerical experiments to evaluate the performance of the proposed methods by comparing them with existing benchmarks. The three methods described in Section 1.1 are considered. First, since there

is no publicly available code for the composite gradient descent algorithm, we implemented the functions in C and wrap them in R (GD). The R source code for the MM-based algorithm (ILAMM) is available at <https://github.com/XiaoouPan/ILAMM>. Finally, the coordinate descent algorithm with second-order local approximation `hqreg` is available on CRAN under the package name `hqreg`.

Throughout the simulation studies, we generate data and compute the entire trajectory of the sequence $\{\lambda_\ell\}_{\ell=1,\dots,100}$, using the same values for all methods. In this study, we compare the computation time (runtime) required to complete all computations for 100 λ values, as well as the log-scaled root mean square error across the λ values. The threshold δ is fixed at 0.5 and is applied uniformly to all methods. Since the definition of the Huber loss function in `hqreg` differs slightly (by a factor of δ), we adjust the values accordingly when using the λ sequence.

The sparse model parameter is inspired by the setting in Gu et al. [2018]. In addition, we consider columns of design matrices sampled from heavy-tailed distributions and/or with highly correlated covariance structures, possibly with a block structure. Specifically, the p -dimensional true parameter β is set as

$$\beta = (2, 0, 1.5, 0, 0.8, 0, 1, 0, 1.75, 0, 0, 0.75, 0, 0, 0.3, \mathbf{0}_{p-16}^\top)^\top \in \mathbb{R}^p.$$

We then generate responses according to $y_i = X_i^\top \beta + e_i$, $i = 1, \dots, n$, where n is the number of samples and $e_i \stackrel{i.i.d.}{\sim} \mathcal{N}(0, 1)$. We consider $n = 100, 500, 1000$ and $p = 100, 500, 1000, 5000$. The columns of the design matrix X_i are generated with covariance matrices $\Sigma_X = (\sigma_{ij})$ according to the following scenarios:

1. Compound \mathcal{N} : $X_i \sim \mathcal{N}(\mathbf{0}_p, \Sigma_X = (1_{\{i=j\}} + 0.8 \times 1_{\{i \neq j\}}))$.
2. AR t_2 : $X_i \sim t_2(\mathbf{0}_p, \Sigma_X = (0.8^{|i-j|}))$.
3. Contaminated AR: $X_i = [X_{1:p-1}, X_p]^\top$, where $X_{1:p-1} \sim \mathcal{N}(\mathbf{0}_{p-1}, \Sigma_X = (0.8^{|i-j|}))$, $X_p \sim t_1$, and $X_{1:p-1} \perp X_p$.
4. Block AR (\mathcal{N}, t_1): $X_i = [X_{1:p/2}, X_{p/2+1:p}]^\top$, where $X_{1:p/2} \sim t_1(\mathbf{0}_{p/2}, \Sigma_X = (0.2^{|i-j|}))$, $X_{p/2+1:p} \sim \mathcal{N}(\mathbf{0}_{p/2}, \Sigma_X = (0.8^{|i-j|}))$, and $X_{1:p/2} \perp X_{p/2+1:p}$.

These scenarios are designed to evaluate the methods under a range of correlation structures and tail behaviors, including both heavy-tailed and mixed distributions. They allow us to assess the robustness of the proposed algorithms in settings that mimic practical high-dimensional data challenges. The simulation is repeated 100 times for each setting.

Figure 2 presents the runtime (CPU seconds) for the same problem across 100 replications. Since the scale of GD is significantly different from the other methods, it is shown separately in Figure 6 in Appendix A. Note that the computational times of the proposed methods are consistently faster than those of the other benchmarks for all combinations of n and p , although the relative performance varies across scenarios. These results highlight the scalability of the proposed methods in high-dimensional regimes.

Figure 3 presents the log-scaled average normalized RMSE. The thick solid lines are the averages of 100 replications at each λ_ℓ , where the shaded areas are 5th and 9th percentile ranges. For all combinations of n and p , we observe that the RMSEs consistently decrease over the lambda sequences, while the other methods struggling, as shown by the radical V-shape curves in their averages. Moreover, using the `hqreg` method, the RMSEs are significantly large compared to the proposed method and other benchmarks. (For sufficiently large n , the performance tends to be better, but they do not provide reliable results in all cases.) By taking into account the data generating process, our method is the most robust and reliable under these challenging scenarios, across different sample sizes and dimensions.

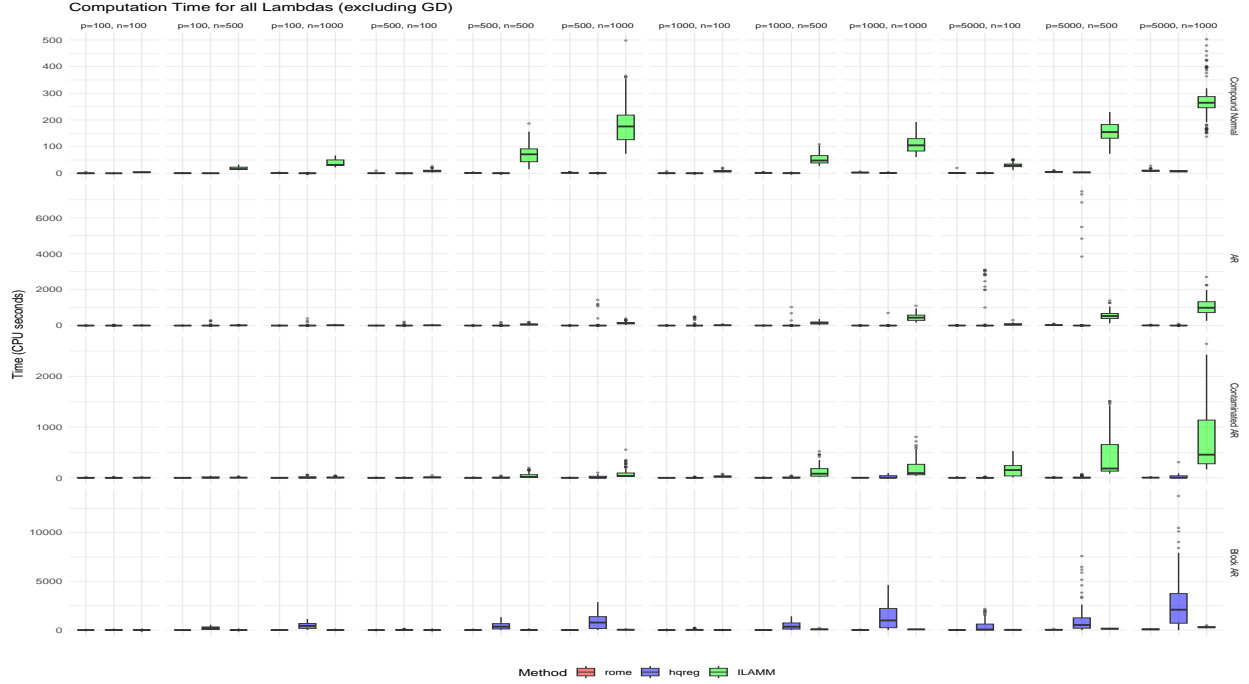


Figure 2: Boxplots of runtimes (CPU seconds) for the same 100 values of λ across 100 replications. Each column corresponds to a different (n, p) setting, and each row corresponds to one of four scenarios for $\{X_i\}$. The proposed method (`rome`) is shown in red, and the benchmarks (`hqreg`, `ILAMM`) are shown in blue and green, respectively. The results from GD are drawn separately.

4.2 Second Numerical Study

We demonstrate the effectiveness of the two computational tricks described in Sections 3.2 and 3.3, implemented in `rome`.

For the first part of the computational tricks, we assess the correctness of the selection rules by comparing (i) the adaptive sequential strong rule (ASR) and (ii) the sequential strong rule (SSR), where the slopes in (17) are set as $M_\ell = 1$ for all ℓ . Following a simulation study in Tibshirani et al. [2012], we check whether ASR or SSR produces any violations. Specifically, along the λ_ℓ paths, we count the number of predictors that exceed the screening rule.

In this experiment, we focus on the model $y_i = X_i^\top \beta + e_i$, $i = 1, \dots, n$, with $e_i \stackrel{i.i.d.}{\sim} \mathcal{N}(0, 1)$. We fix $n = 100$ and set $p = 100, 500, 1000$. For the p -dimensional true parameter β , ten percent of the entries are randomly set to 1, with the remaining entries set to 0. The rows of the design matrix are then generated as follows:

5. **AR t_4 :** $X_i \sim t(\mathbf{0}_p, \Sigma_X = (\rho^{|i-j|}))$.
6. **Block AR (\mathcal{N}, \mathcal{N}):** $X_i = [X_{1:p/2}, X_{p/2+1:p}]^\top$, where $X_{1:p/2} \sim \mathcal{N}(\mathbf{0}_{p/2}, \Sigma_X = (\rho_1^{|i-j|}))$, $X_{p/2+1:p} \sim \mathcal{N}(\mathbf{0}_{p/2}, \Sigma_X = (\rho_2^{|i-j|}))$, and $X_{1:p/2} \perp X_{p/2+1:p}$.

Here, $\rho \in \{0, 0.8\}$ and $(\rho_1, \rho_2) \in \{(0.0, 0.8), (0.4, 0.8)\}$, where we call them types 1 and 2, respectively, for each data generating process. Each setup is repeated 100 times.

The results are shown in Figure 4. Note that while SSR tends to increase as the dimension p grows, partic-

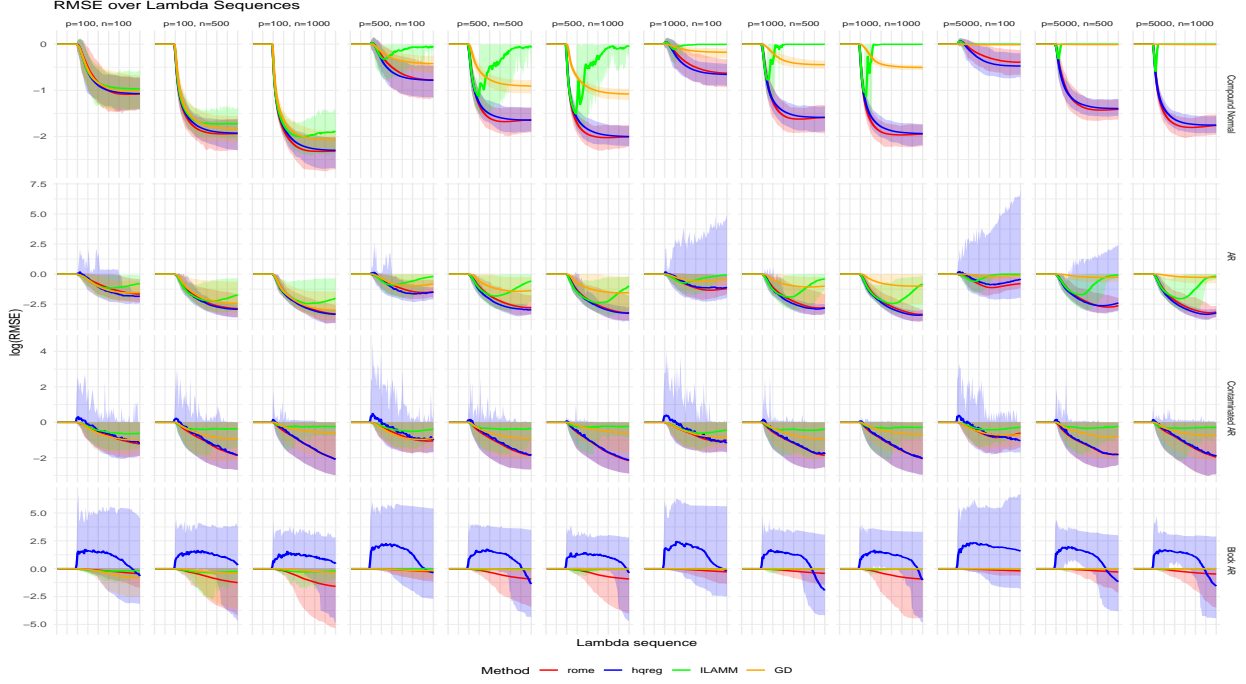


Figure 3: Average normalized RMSE for the same 100 values of λ across 100 replications. The mean RMSEs are shown as solid lines, and the shaded areas indicate the 5th and 95th percentile ranges of RMSEs. Each column corresponds to a different (n, p) setting, and each row corresponds to one of four scenarios of $\{X_i\}$. The proposed method (**rome**) is shown in red, and the benchmarks (**hqreg**, **ILAMM**, **GD**) are shown in blue, green, and orange, respectively.

ularly for smaller λ values, ASR remains zero across all λ values, regardless of the dimension. Interestingly, the proportion of violations depends on the values of λ and the problem dimension, but is less affected by the scenario. These results demonstrate that ASR provides a more reliable and stable screening rule compared to SSR, especially in high-dimensional settings.

The second part of the investigation focuses on the effectiveness of checking the KKT conditions in the proposed algorithm. In these simulations, no screening rules are applied. We compare the running times between (i) applying KKT condition checks and (ii) not applying them. We again use the model $y_i = X_i^\top \beta + e_i$, $i = 1, \dots, n$, $e_{i,t} \stackrel{i.i.d.}{\sim} \mathcal{N}(0, 1)$. Here, we fix $\rho = 0.4$ and $(\rho_1, \rho_2) = (0.2, 0.8)$ for data generating models 5 and 6, respectively. By following the simulation setup for time comparison in Yi and Huang [2017], we use

$$\beta_j = (-1)^j \exp(-(j-1)/10), \quad j = 1, \dots, p,$$

and choose $p = 50, 100, 200, 500, 1000$ and $n = 100, 500$. The reported results are the averages of 100 runs of CPU time (in seconds).

The results are shown in Table 1. Note that using the KKT condition check is highly beneficial compared to not using it, across all combinations of n and p , as well as across different data generating scenarios. Interestingly, the runtime tends to increase approximately proportionally with both n and p in both cases. While the increase in runtime with respect to p appears modest, the increase with respect to n is likely due to the sorting operations included in the algorithm.

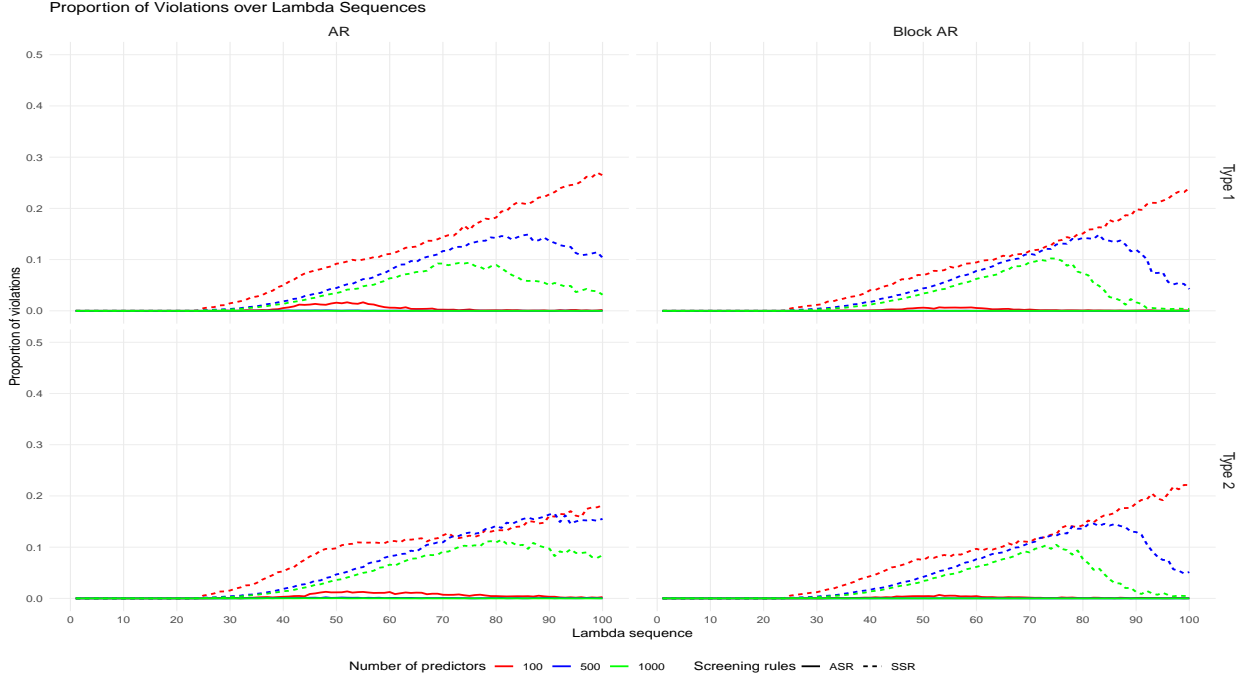


Figure 4: Average proportion of violations among the total number of variables across 100 replications under different rules (ASR and SSR) with `rome`. The columns correspond to scenario 1 (AR) and scenario 2 (Block AR), while the rows present the results for type 1 and type 2. Within each panel, six cases are displayed; solid and dotted lines represent ASR and SSR, respectively, and the colors red, blue, and green correspond to $p = 100, 500$, and 1000 , respectively.

4.3 Real Data Application

Finally, we present an application in which the characteristics of the dataset resemble the scenarios considered in the simulation studies. We analyze a dataset from electron-probe X-ray microanalysis of $n = 180$ archaeological glass vessels Janssens et al. [1998], where each vessel is represented by a spectrum across 1,920 frequencies and the contents of 13 chemical compounds are recorded. Our focus is on predicting the content of the 13th compound (PbO) using the spectral frequencies as predictors. Since values below frequency 15 and above 500 are nearly zero with little variability, we only retain frequencies 15–500, resulting in $p = 486$ predictors. This dataset has been used in studies of high-dimensional robust regression [e.g., Maronna, 2011; Smucler and Yohai, 2017; Loh, 2021].

As seen in the left panel of Figure 5, the dataset contains clusters of clear outliers, which give rise to a block structure in the design matrix. This structure is clearly reflected in the covariance matrix, as shown in the right panel of Figure 5. The presence of these outliers and the resulting block correlation patterns highlight the need for methods that can handle both heavy-tailed errors and high dependence between predictors.

First, we illustrate cross-validation results, similar to those shown in Wu and Lange [2008]. We select the optimal λ via cross-validation by minimizing (i) the null deviance, (ii) the mean absolute error, and (iii) the root mean squared error. The results are displayed in Figure 7 in Appendix A. Note that the three metrics do not show substantial differences, and all exhibit a weak U-shape across the λ values. The two thick lines indicate the λ values chosen: one minimizes the metric, and the other represents the largest λ for which the cross-validated error is within one standard error from the minimum. This approach is widely used when interpreting cross-validation results [e.g., Friedman et al., 2010].

		KKT check	$p = 50$	$p = 100$	$p = 200$	$p = 500$	$p = 1000$
AR	$n = 100$	Applied	0.187	0.331	0.598	1.174	1.449
		N/A	0.915	1.857	3.850	10.537	20.566
	$n = 500$	Applied	0.676	0.906	1.404	3.365	6.600
		N/A	4.695	9.685	19.350	52.038	106.008
Block AR	$n = 100$	Applied	0.171	0.294	0.648	0.929	1.025
		N/A	0.943	1.826	3.807	10.220	21.209
	$n = 500$	Applied	0.592	0.796	1.172	2.741	5.559
		N/A	4.756	9.823	19.786	51.976	104.985

Table 1: Average runtimes (CPU seconds) for the same 100 values of λ across 100 replications. The cases where KKT checking is applied (Applied) and not applied (NA) are compared.

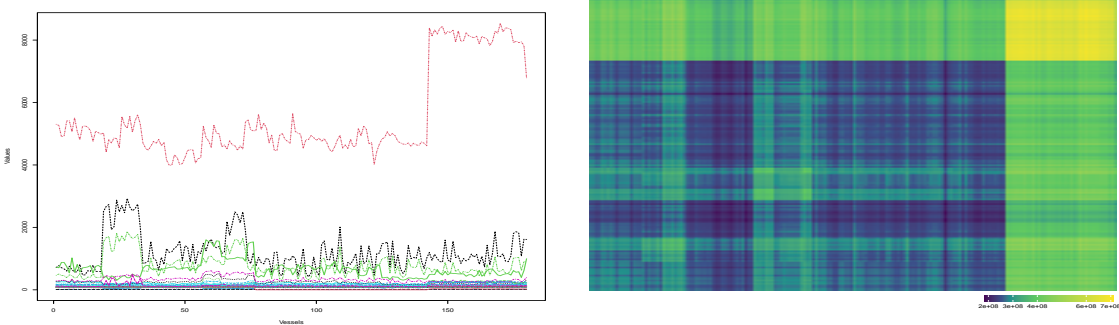


Figure 5: Plots of the X-ray microanalysis over randomly chosen 30 frequencies (left panel) and the sample covariance matrix of the covariates (right panel).

Second, we report the number of selected nonzero coefficients based on the entire sample, as well as the predictive performance, following a similar approach used in other penalized robust regression studies [e.g., Peng and Wang, 2015; Gu et al., 2018]. Specifically, for prediction tasks, we generate 50 random partitions of the data, with each partition containing 120 glass vessels in the training set I_{train} and 60 vessels in the validation set I_{val} . For each partition, we fit the model using 5-fold cross-validation on the training set, using the null deviance as the selection criterion, and compute the prediction error on the validation set as

$$\frac{1}{60} \sum_{i \in I_{\text{val}}} \rho_\delta(y_i - X_i^\top \hat{\beta}(I_{\text{test}})).$$

We use three thresholds, $\delta = 0.5, 1.0$, and 1.5 .

The results are displayed in Table 2. Across the three values of δ , we observe that the number of nonzero coefficients selected from the entire dataset varies, with $\delta = 1.0$ yielding the largest model. When evaluating the 50 random partitions, the average number of selected nonzeros is generally higher than that obtained from the full dataset, reflecting variability across the training subsets. The corresponding prediction errors on the validation sets are relatively low for all δ values, with the smallest error observed at $\delta = 0.5$. Overall, these results suggest that Huber regression performs robustly across different choices of δ , balancing model sparsity and predictive accuracy.

5 Discussion

The proposed algorithm achieves superior performance compared to benchmark methods in challenging scenarios with ill-conditioned Hessian matrices caused by highly correlated covariates and heavy-tailed dis-

Model	All Data # of nonzeros	Random Partition	
		Average # of nonzeros	Prediction Error
$\delta = 0.5$	131	200.7 (78.612)	0.015 (0.006)
$\delta = 1.0$	242	239.1 (83.068)	0.021 (0.008)
$\delta = 1.5$	131	200.2 (95.115)	0.030 (0.008)

Table 2: Analysis of the X-ray microanalysis glass vessels data reported in Janssens et al. [1998] by Huber regression with three different values of δ . For the random partition, the mean and standard deviation (in parentheses) for the 50 replications are reported.

tributions, offering gains in both computation time and estimation accuracy. In these settings, the method not only reduces computational time but also achieves lower estimation error, highlighting its robustness and efficiency. It comes with theoretical convergence guarantees and practical acceleration strategies, such as an adaptive sequential strong screening rule and KKT condition checks. To our knowledge, this is the first first-order coordinate descent method for composite function minimization with both nonsmooth loss and penalty functions, validated through theory and numerical experiments.

Despite these advances, several directions remain for future research. First, the method cannot be directly extended to robust loss functions such as Cauchy or Tukey, since their interval-dependent slopes make index tracking prohibitively complex. Further research is needed to develop effective approximations for these cases. In addition, while the screening rule substantially reduces computation time, a deeper investigation of its properties remains for future work. Finally, extending the method to the elastic net penalty [Zou and Hastie, 2005] might be practically straightforward, but establishing convergence guarantees under the same proof strategy remains an open challenge.

Acknowledgements

SB acknowledges partial support from NSF CAREER award DMS-2239102, NSF awards DMS-1812128, DMS-2210675, and NIH awards R01GM135926, R21NS120227.

Data Availability Statement

The R package `rome` and the code used for the simulation studies and the data application in Section 4 are available on GitHub at <https://github.com/yk748/rome>. The dataset used in Section 4.3 is also provided in the repository.

A Additional Figures

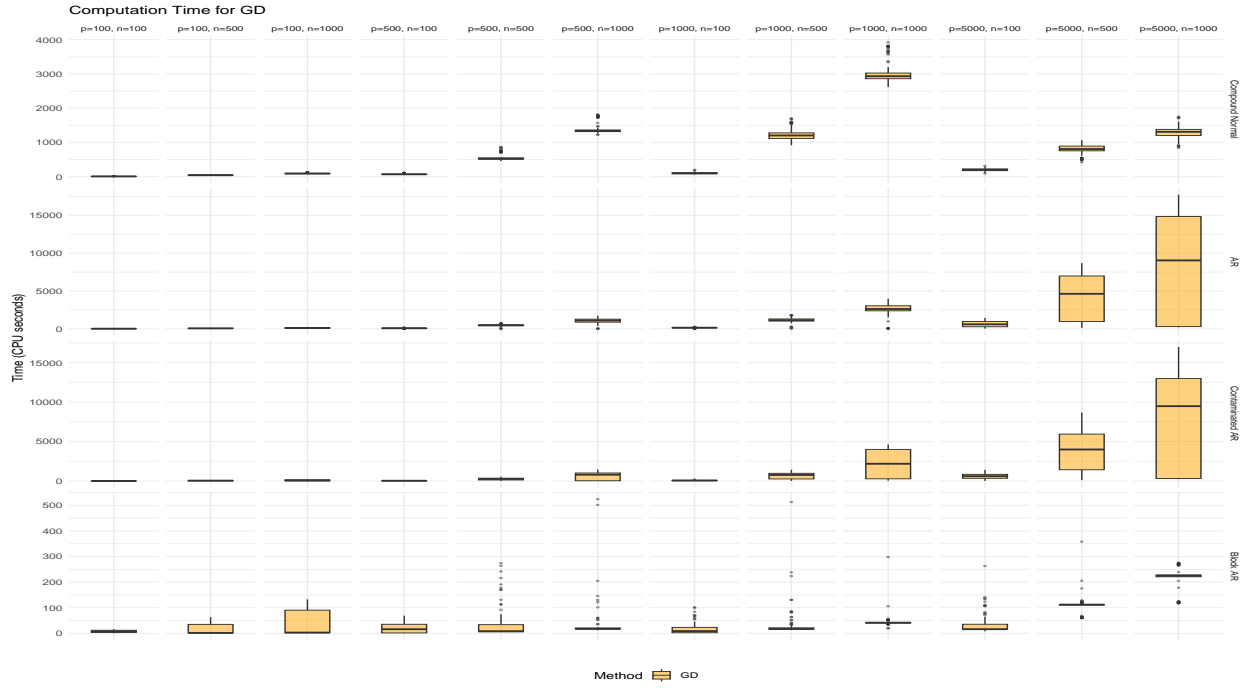


Figure 6: Boxplots of runtimes (CPU seconds) for GD.

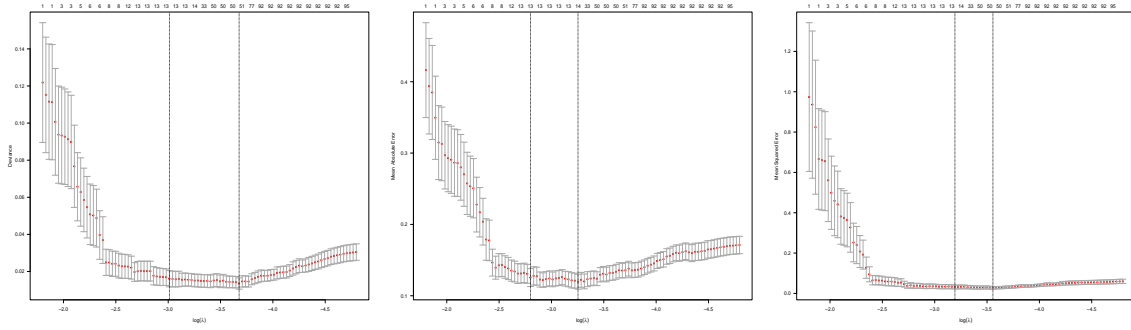


Figure 7: Plot of 10-fold cross-validation error and number of predictors versus 100 values of λ for $\delta = 0.5$. The evaluation criteria used are null deviance (left panel), mean absolute error (middle panel), and root mean square error (right panel), respectively.

B Proof of Proposition 2.1

In this section, we present the necessary details from Saha and Tewari [2013] to provide a complete understanding of Proposition 2.1 in Section 2.3.

Denote by $\{u^{(k)}\}$, $\{v^{(k)}\}$, and $\{z^{(k)}\}$ the solution paths of the regularized Huber regression obtained via gradient descent (GD), gradient-based coordinate descent (CGD; e.g., Tseng and Yun [2009]), and coordinate minimization (CM), respectively, where our proposed method belongs to the last category.

GD: Suppose that we solve a given penalized Huber regression problem (1). The GD uses the update at each iteration described in (4): With $\eta = L$,

$$u^{(k+1)} = S_{\lambda/L} \left(u^{(k)} - \frac{1}{L} \nabla f(u^{(k)}) \right).$$

CGD: For each k , the CGD updates the variables coordinatewise as

$$\begin{aligned} v_1^{(k)} &= S_{\lambda/L} \left(v_1^{(k-1)} - t_{k,1} \nabla f(v_1^{(k-1)}, v_2^{(k-1)}, v_3^{(k-1)}, \dots, v_p^{(k-1)}) \right), \\ v_2^{(k)} &= S_{\lambda/L} \left(v_2^{(k-1)} - t_{k,2} \nabla f(v_1^{(k)}, v_2^{(k-1)}, v_3^{(k-1)}, \dots, v_p^{(k-1)}) \right), \\ &\vdots \\ v_p^{(k)} &= S_{\lambda/L} \left(v_p^{(k-1)} - t_{k,p} \nabla f(v_1^{(k)}, v_2^{(k)}, v_3^{(k)}, \dots, v_p^{(k-1)}) \right). \end{aligned}$$

where $t_{k,1}, t_{k,2}, t_{k,3}, \dots$ are stepsizes.

CM: For each k , the CM updates the variables coordinatewise as

$$\begin{aligned} z_1^{(k)} &\in \arg \min_{z_1 \in \mathbb{R}} F(z_1, z_2^{(k-1)}, z_3^{(k-1)}, \dots, z_p^{(k-1)}), \\ z_2^{(k)} &\in \arg \min_{z_2 \in \mathbb{R}} F(z_1^{(k)}, z_2, z_3^{(k-1)}, \dots, z_p^{(k-1)}), \\ &\vdots \\ z_p^{(k)} &\in \arg \min_{z_p \in \mathbb{R}} F(z_1^{(k)}, z_2^{(k)}, z_3^{(k)}, \dots, z_p). \end{aligned}$$

The following is the key concept of the proof when the shrinkage operator (5) is monotone increasing.

Definition B.1. A vector α is a supersolution (subsolution, respectively) if and only if, for some $\tau > 0$,

$$\alpha \geq S_{\lambda/\tau} \left(\alpha - \frac{\nabla F(x)}{\tau} \right), \tag{B.1}$$

$$\alpha \leq S_{\lambda/\tau} \left(\alpha - \frac{\nabla F(x)}{\tau} \right). \tag{B.2}$$

Note that if the equality holds, i.e., $\alpha = S_{\lambda/\tau} \left(\alpha - \frac{\nabla F(\alpha)}{\tau} \right)$, then α is a minimizer, and the converse is also true, since from the KKT condition,

$$0 \in [\nabla f(\alpha)]_j + \lambda \text{sign}(\alpha_j)$$

for all j . From Definition B.1, any minimizer of F is automatically both a supersolution and a subsolution. However, if this were the only case, then results that assume the starting point is a supersolution or subsolution would be trivial. To show the concepts are not degenerate, we give the following lemma; its proof is

essentially the same as in Saha and Tewari [2013] but uses the fact that the Huber loss (2) is differentiable with a Lipschitz gradient L_H defined in Proposition 2.1.

Lemma B.1. *Let f be the Huber loss (2) and $\nabla f(\alpha)$ is L_H -Lipschitz. A sufficient condition for α to be a supersolution (subsolution, respectively) is $[\nabla f(\alpha)]_j \geq \lambda$ (respectively, $[\nabla f(\alpha)]_j \leq \lambda$) for all j .*

Proof. Fix the j^{th} coordinate. If $[\nabla f(\alpha)]_j \geq \lambda$, then

$$\alpha_j - \frac{1}{L_H} [\nabla f(\alpha)]_j \leq \alpha_j - \frac{\lambda}{L_H}.$$

Since the soft-thresholding operator (5) is nondecreasing,

$$S_{\lambda/L_H} \left(\alpha_j - \frac{1}{L_H} [\nabla f(\alpha)]_j \right) \leq S_{\lambda/L_H} \left(\alpha_j - \frac{\lambda}{L_H} \right) \leq \alpha_j - \frac{\lambda}{L_H} \leq \alpha_j.$$

Thus, $\alpha \geq S_{\lambda/L_H}(\alpha - \nabla f(\alpha)/L_H)$, so α is a supersolution. The subsolution case can be analogously shown. \square

Because the Huber loss has a globally Lipschitz gradient and the soft-thresholding operator (5) has the monotonicity and shrinkage properties used above, this implies that the supersolution and subsolution concepts are nondegenerate in the Huber loss case.

The following are the technical lemmas to prove the key results below. We omit the proofs as they are the same as those in Saha and Tewari [2013].

Lemma B.2 (cf. Lemmas 4.3, 4.4, 7.1, 8.1, and 8.2 in Saha and Tewari [2013]).

(a) *If the inequality (B.1) holds for some $\tau > 0$, then it holds for all $\tau > 0$. A similar result holds for (B.2).*

(b) *If α is a supersolution (subsolution, respectively), then for any j , the function*

$$\tau \mapsto S_{\lambda/\tau} \left(\alpha_j - \frac{[\nabla F(x)]_j}{\tau} \right)$$

is monotonically nondecreasing (nonincreasing, respectively) on $(0, \infty)$.

(c) *Fix $k \geq 0$, $j = 1, \dots, p$. For the CM updates, let $g_j(\alpha_j) = f_j(\alpha_j; z_j^{(k,j-1)})$. The nontrivial update can be written as*

$$z_j^{(k,j)} = S_{\lambda/\tau_j} \left(z_j^{(k,j-1)} - \frac{[\nabla f(z_j^{(k,j-1})]_j}{\tau_j} \right),$$

where τ_j is defined in (16).

(d) *If v is a supersolution and $v \leq u$ or v is a subsolution and $v \geq u$, then $F(v) \leq F(u)$.*

Statements (a) and (b) show that the supersolution and subsolution concepts are defined for all τ and are scale-invariant. In addition, statement (c) implies that, when combined with Proposition 2.1 that τ is upper-bounded, the CM-type solutions are also comparable with those obtained from CGD. Finally, statement (d) allows us to compare solutions from different optimizers by mapping them to their respective objective functions.

Proof. The proofs of (a), (b), and (d) remain the same as those in Lemmas 4.3, 4.4, 8.1, and 8.2 of Saha and Tewari [2013]. Note that by the definition of $g_j(\alpha_j)$ in the statement and τ_j defined as in (16), $z_j^{(k,j)}$ is the minimizer of the form $g_j(\alpha_j) + \lambda|\alpha_j|$. Then we have

$$0 \in g'_j(z_j^{(k,j)}) + \lambda \text{sign}(z_j^{(k,j)}) = \tau_j(z_j^{(k,j)} - z_j^{(k,j-1)}) + g'_j(z_j^{(k,j-1)}) + \lambda \text{sign}(z_j^{(k,j)}) \quad (\text{B.3})$$

First, if $z_j^{(k,j)} = 0$, then from (B.3),

$$\begin{aligned} g'_j(z_j^{(k,j)}) - \lambda &\leq 0 \leq g'_j(z_j^{(k,j)}) + \lambda \\ \Leftrightarrow -\tau_j z_j^{(k,j-1)} + g'_j(z_j^{(k,j-1)}) - \lambda &\leq 0 \leq -\tau_j z_j^{(k,j-1)} + g'_j(z_j^{(k,j-1)}) + \lambda \\ \Leftrightarrow z_j^{(k,j-1)} - \frac{g'_j(z_j^{(k,j-1)})}{\tau_j} - \frac{\lambda}{\tau_j} &\leq 0 \leq z_j^{(k,j-1)} - \frac{g'_j(z_j^{(k,j-1)})}{\tau_j} + \frac{\lambda}{\tau_j}, \end{aligned}$$

which implies

$$0 = S_{\lambda/\tau_j} \left(z_j^{(k,j-1)} - \frac{g'_j(z_j^{(k,j-1)})}{\tau_j} \right).$$

If $z_j^{(k,j)} > 0$, from $g'_j(z_j^{(k,j)}) + \lambda = 0$ in (B.3), we have

$$\begin{aligned} 0 &= \tau_j(z_j^{(k,j)} - z_j^{(k,j-1)}) + g'_j(z_j^{(k,j-1)}) + \lambda \\ \Leftrightarrow z_j^{(k,j)} &= z_j^{(k,j-1)} - \frac{g'_j(z_j^{(k,j-1)})}{\tau_j} - \frac{\lambda}{\tau_j} = S_{\lambda/\tau_j} \left(z_j^{(k,j-1)} - \frac{g'_j(z_j^{(k,j-1)})}{\tau_j} \right). \end{aligned}$$

The case of $z_j^{(k,j)} < 0$ can be shown analogously. \square

The following is the key result from the solutions of GD, CGD, and CM.

Lemma B.3 (cf. Propositions 5.1, 6.1, and Lemma 7.2 in Saha and Tewari [2013]). *Assume that for a variable α the operator $\alpha \mapsto \alpha - \frac{\nabla f(\alpha)}{L}$ is monotonically increasing.*

(a) *If $u^{(0)}$ is a supersolution (subsolution, respectively) and $\{u^{(k)}\}_{k=1,2,\dots}$ is the sequence of iterates generated by the GD algorithm, then for all $k \geq 0$,*

$$u^{(k+1)} \leq u^{(k)} \text{ \& } u^{(k)} \text{ is a supersolution } (u^{(k+1)} \geq u^{(k)} \text{ \& } u^{(k)} \text{ is a subsolution, respectively}).$$

(b) *If $v^{(0)}$ is a supersolution (subsolution, respectively) and $\{v^{(k)}\}_{k=1,2,\dots}$ is the sequence of iterates generated by the CGD algorithm, then for all $k \geq 0$,*

$$v^{(k+1)} \leq v^{(k)} \text{ \& } v^{(k)} \text{ is a supersolution } (v^{(k+1)} \geq v^{(k)} \text{ \& } v^{(k)} \text{ is a subsolution, respectively}).$$

(c) *If $z^{(0)}$ is a supersolution (subsolution, respectively) and $\{z^{(k)}\}_{k=1,2,\dots}$ is the sequence of iterates generated by the CM algorithm, then for all $k \geq 0$,*

$$z^{(k+1)} \leq z^{(k)} \text{ \& } z^{(k)} \text{ is a supersolution } (z^{(k+1)} \geq z^{(k)} \text{ \& } z^{(k)} \text{ is a subsolution, respectively}).$$

Proof. The proofs of (a) and (b) remain the same as those in Propositions 5.1 and 6.1 of Saha and Tewari [2013]. For (c), first claim that

$$z_j^{(k,j)} \leq z_j^{(k,j-1)} = z_j^{(k)}.$$

From the statements (b) and (c) in Lemma B.2,

$$z_j^{(k,j)} = S_{\lambda/\tau_j} \left(z_j^{(k,j-1)} - \frac{g'_j(z_j^{(k,j-1)})}{\tau_j} \right) \leq S_{\lambda/L_H} \left(z_j^{(k,j-1)} - \frac{g'_j(z_j^{(k,j-1)})}{L_H} \right) \leq z_j^{(k)},$$

where the last inequality can be shown through $z^{(k,j-1)} \leq z^{(k)}$ for all j . Next, from (B.3), by using $g'_j(z_j^{(k,j)}) + \lambda = 0$, we have

$$\begin{aligned} g'_j(z_j^{(k,j)}) &= \tau_j(z_j^{(k,j)} - z_j^{(k,j-1)}) + g'_j(z_j^{(k,j-1)}) \\ \Leftrightarrow z_j^{(k,j)} - \frac{g'_j(z_j^{(k,j)})}{\tau_j} &= z_j^{(k,j-1)} - \frac{g'_j(z_j^{(k,j-1)})}{\tau_j} \\ \Leftrightarrow S_{\lambda/\tau_j} \left(z_j^{(k,j)} - \frac{g'_j(z_j^{(k,j)})}{\tau_j} \right) &= S_{\lambda/\tau_j} \left(z_j^{(k,j-1)} - \frac{g'_j(z_j^{(k,j-1)})}{\tau_j} \right) = z_j^{(k,j)}. \end{aligned}$$

From $z^{(k,j-1)} \geq z^{(k,j)}$ and $z_{j'}^{(k,j)} = z_{j'}^{(k,j-1)}$ for $j' \neq j$, we have

$$g'_{j'}(z^{(k,j-1)}) - g'_{j'}(z^{(k,j)}) \leq L_H(z_{j'}^{(k,j-1)} - z_{j'}^{(k,j)}) = 0$$

for all $j' \neq j$. This implies that

$$\begin{aligned} z_{j'}^{(k,j-1)} - \frac{g'_{j'}(z_{j'}^{(k,j-1)})}{\tau'_{j'}} &\geq z_{j'}^{(k,j)} - \frac{g'_{j'}(z_{j'}^{(k,j)})}{\tau'_{j'}} \\ \Leftrightarrow S_{\lambda/\tau'_{j'}} \left(z_{j'}^{(k,j-1)} - \frac{g'_{j'}(z_{j'}^{(k,j-1)})}{\tau'_{j'}} \right) &\geq S_{\lambda/\tau'_{j'}} \left(z_{j'}^{(k,j)} - \frac{g'_{j'}(z_{j'}^{(k,j)})}{\tau'_{j'}} \right) \\ \Rightarrow z_{j'}^{(k,j)} = z_{j'}^{(k,j-1)} &\geq S_{\lambda/\tau'_{j'}} \left(z_{j'}^{(k,j-1)} - \frac{g'_{j'}(z_{j'}^{(k,j-1)})}{\tau'_{j'}} \right) \geq S_{\lambda/\tau'_{j'}} \left(z_{j'}^{(k,j)} - \frac{g'_{j'}(z_{j'}^{(k,j)})}{\tau'_{j'}} \right). \end{aligned}$$

This holds for all $j' = 1, \dots, p$. Hence, by using statements (a) and (b) in Lemma B.3 and the fact that $\tau_{j'} \leq L_H$ for all j' , we have

$$z^{(k,j)} \geq S_{\lambda/L_H} \left(z^{(k,j)} - \frac{\nabla f(z^{(k,j)})}{L_H} \right).$$

This implies that $z^{(k,j)}$ is a supersolution. The case of subsolution can be shown analogously. \square

The following allows us to compare the solutions of GD, CGD, and CM that satisfy the given conditions.

Lemma B.4 (cf. Theorems 6.2 and 7.3 in Saha and Tewari [2013]). *Consider $u^{(0)}, v^{(0)}, z^{(0)}, \{u^{(k)}\}_{k=1,2,\dots}, \{v^{(k)}\}_{k=1,2,\dots}$, and $\{z^{(k)}\}_{k=1,2,\dots}$ are defined in Lemma B.3.*

- (a) *If $u^{(0)} = v^{(0)}$ are supersolutions, then for all $k \geq 0$, $v^{(k)} \leq u^{(k)}$. Conversely, if $u^{(0)} = v^{(0)}$ are subsolutions, then for all $k \geq 0$, $v^{(k)} \geq u^{(k)}$.*
- (b) *If $v^{(0)} = z^{(0)}$ are supersolutions, then for all $k \geq 0$, $z^{(k)} \leq v^{(k)}$. Conversely, if $u^{(0)} = v^{(0)}$ are subsolutions, then for all $k \geq 0$, $z^{(k)} \geq v^{(k)}$.*

Proof. The proof of (a) remains the same as that in Theorems 6.2 of Saha and Tewari [2013]. For (b), we focus on the nontrivial update. Note that for fixed k ,

$$\begin{aligned} z_j^{(k,j)} &= S_{\lambda/\tau} \left(z_j^{(k,j-1)} - \frac{[\nabla f(z^{(k,j-1)})]_j}{\tau_j} \right) \leq S_{\lambda/L_H} \left(z_j^{(k,j-1)} - \frac{[\nabla f(z^{(k,j-1)})]_j}{L_H} \right) \\ &\leq S_{\lambda/L_H} \left(v_j^{(k,j-1)} - \frac{[\nabla f(v^{(k,j-1)})]_j}{L_H} \right) = v^{(k,j)}. \end{aligned}$$

Using mathematical induction, the proof can be completed, as the remaining steps are identical to those in Theorem 7.3 of Saha and Tewari [2013]. \square

Finally, the following result directly implies the convergence of the proposed method.

Lemma B.5 (cf. Theorem 8.3 in Saha and Tewari [2013]). *Starting from the same initial point $u^{(0)} = v^{(0)} = z^{(0)}$, the solution paths $\{u^{(k)}\}, \{v^{(k)}\}, \{z^{(k)}\}$ produced by GD, CGD, and CM at the k^{th} iteration satisfy*

$$F(z^{(k)}) \leq F(v^{(k)}) \leq F(u^{(k)}) \leq F(u^*) + \frac{L_H \|u^{(0)} - u^*\|^2}{2k}, \quad (\text{B.4})$$

where u^* denotes the optimal solution and L is the Lipschitz constant, given by the problem.

Proof. The first and second inequalities in (B.4) follow immediately by combining statement (a) of Lemma B.4 with statement (d) of Lemma B.2, and statement (b) of Lemma B.4 with statement (d) of Lemma B.2, respectively. The last inequality holds by the standard argument of the GD algorithm [see also Theorem 3.1 in Beck and Teboulle, 2009]. \square

Now we can complete the proof of Proposition 2.1.

Proof of Proposition 2.1. We now claim that τ_j is bounded by the largest achievable Lipschitz constant L_H , which is itself bounded by $\frac{1}{n} \text{eig}_{\max}(X^T X)$. This ensures that the coordinate derivatives $[\nabla F(\alpha)]_j$ for the updating coordinate, as used in Lemmas B.2, B.3, and B.4, are always well-defined. Therefore, from the pairwise comparisons (B.4) between the solutions in Lemma B.5, it follows that (15) in Proposition 2.1 holds.

We drop some k in indices for simplicity. It remains to show that both τ_j and L_H are bounded by $\frac{1}{n} \text{eig}_{\max}(X^T X)$. First, from the definition of $f(\beta)$ in (12), we have

$$\nabla f(\beta) = -\frac{1}{n} X^T \psi(r(\beta)),$$

where $r_i(\beta) = y_i - X_i^T \beta$, $i = 1, \dots, n$, and $\psi(u) = (\rho'_\delta(u_1), \rho'_\delta(u_2), \dots, \rho'_\delta(u_p))^T \in \mathbb{R}^p$ for $u \in \mathbb{R}^p$. For a pair of $\beta, \beta' \in \mathbb{R}^p$, by using the fact that $|\rho'_\delta(u_i) - \rho'_\delta(v_i)| \leq |u_i - v_i|$ for any $u_i, v_i \in \mathbb{R}$ implies $\|\psi(u) - \psi(v)\|_2 \leq \|u - v\|_2$ for $u, v \in \mathbb{R}^p$, we have

$$\begin{aligned} \|\nabla f(\beta) - \nabla f(\beta')\|_2 &= \frac{1}{n} \|X^T (\psi(r(\beta)) - \psi(r(\beta')))\|_2 \leq \frac{1}{n} \|X^T\|_2 \|\psi(r(\beta)) - \psi(r(\beta'))\|_2 \\ &\leq \frac{1}{n} \|X^T\|_2 \|X\|_2 \|\beta - \beta'\|_2 = \frac{1}{n} \text{eig}_{\max}(X^T X) \|\beta - \beta'\|_2, \end{aligned}$$

where the last inequality holds since $\|r(\beta) - r(\beta')\|_2 = \|X(\beta - \beta')\|_2$. Hence, $L_H \leq \frac{1}{n} \text{eig}_{\max}(X^T X)$. Now, we claim that $\tau_j \leq \frac{1}{n} \text{eig}_{\max}(X^T X)$ for all j . For fixed j , define

$$g(\alpha) = g(\beta_{-j}, \alpha) = \frac{1}{n} \sum_{i=1}^n \rho_\delta \left(y_i - \sum_{k \neq j} X_{ik} \beta_k - X_{ij} \alpha \right).$$

Note that $g'(\alpha) = -\frac{1}{n} \sum_{i=1}^n X_{ij} [\psi(r_i(\alpha))]_j$ and $g''_j(\alpha) = \frac{1}{n} \sum_{i=1}^n X_{ij}^2 [\psi'(r_i(\alpha))]_j = \frac{1}{n} \sum_{i=1}^n X_{ij}^2$ since $[\psi'(u)]_j \in \{0, 1\}$. Then for all α ,

$$0 \leq g'(\alpha) \leq \frac{1}{n} \sum_{i=1}^n X_{ij}^2 \leq \frac{1}{n} \text{eig}_{\max}(X^T X).$$

Recall the definition of τ_j in (16). For a pair of $\alpha, \alpha' \in \mathbb{R}$, $\alpha \neq \alpha'$, such that

$$\tau_j = \frac{g'(\alpha) - g'(\alpha')}{\alpha - \alpha'},$$

there exists $\xi \in (\alpha, \alpha')$ such that $g''(\xi) = \tau_j$ by the mean value theorem. Hence,

$$\tau_j \leq \sup_{\xi} g''(\xi) \leq \frac{1}{n} \text{eig}_{\max}(X^T X),$$

which completes the proof. \square

References

Avella Medina, M. and Ronchetti, E. (2015). Robust statistics: A selective overview and new directions. *Wiley Interdisciplinary Reviews: Computational Statistics*, 7(6):372–393.

Beck, A. (2017). *First-Order Methods in Optimization*. SIAM.

Beck, A. and Teboulle, M. (2009). A fast iterative shrinkage-thresholding algorithm for linear inverse problems. *SIAM Journal on Imaging Sciences*, 2(1):183–202.

Chen, X. (2012). Smoothing methods for nonsmooth, nonconvex minimization. *Mathematical Programming*, 134(1):71–99.

Clarke, F. H. (1990). *Optimization and Nonsmooth Analysis*, volume 5. SIAM.

Cormen, T. H., Leiserson, C. E., Rivest, R. L., and Stein, C. (2022). *Introduction to Algorithms*. MIT Press.

Fan, J., Liu, H., Sun, Q., and Zhang, T. (2018). I-LAMM for sparse learning: Simultaneous control of algorithmic complexity and statistical error. *The Annals of Statistics*, 46(2):814.

Friedman, J., Hastie, T., Höfling, H., and Tibshirani, R. (2007). Pathwise coordinate optimization. *The Annals of Applied Statistics*, 1(2):302–332.

Friedman, J. H., Hastie, T., and Tibshirani, R. (2010). Regularization paths for generalized linear models via coordinate descent. *Journal of Statistical Software*, 33:1–22.

Gu, Y., Fan, J., Kong, L., Ma, S., and Zou, H. (2018). ADMM for high-dimensional sparse penalized quantile regression. *Technometrics*, 60(3):319–331.

Hampel, F. R., Ronchetti, E. M., Rousseeuw, P. J., and Stahel, W. A. (2011). *Robust Statistics: The Approach Based on Influence Functions*. John Wiley & Sons.

Hastie, T., Tibshirani, R., and Wainwright, M. (2015). Statistical learning with sparsity. *Monographs on Statistics and Applied Probability*, 143(143):8.

Huber, P. J. and Ronchetti, E. M. (2011). *Robust Statistics*. John Wiley & Sons.

Janssens, K. H., Deraedt, I., Schalm, O., and Veeckman, J. (1998). Composition of 15–17th century archaeological glass vessels excavated in antwerp, belgium. In *Modern Developments and Applications in Microbeam Analysis*, pages 253–267. Springer.

Kim, S. and Basu, S. (2025). A pathwise coordinate descent algorithm for LASSO penalized quantile regression. *arXiv preprint arXiv:2502.12363*.

Loh, P.-L. (2017). Statistical consistency and asymptotic normality for high-dimensional robust m -estimators. *The Annals of Statistics*, pages 866–896.

Loh, P.-L. (2021). Scale calibration for high-dimensional robust regression. *Electronic Journal of Statistics*, 15(2):5933–5994.

Loh, P.-L. (2024). A theoretical review of modern robust statistics. *Annual Review of Statistics and Its Application*, 12.

Maronna, R. A. (2011). Robust ridge regression for high-dimensional data. *Technometrics*, 53(1):44–53.

Maronna, R. A., Martin, R. D., Yohai, V. J., and Salibián-Barrera, M. (2019). *Robust Statistics: Theory and Methods (with R)*. John Wiley & Sons.

Mifflin, R. (1977). Semismooth and semiconvex functions in constrained optimization. *SIAM Journal on Control and Optimization*, 15(6):959–972.

Nesterov, Y. (2013a). Gradient methods for minimizing composite functions. *Mathematical Programming*, 140(1):125–161.

Nesterov, Y. (2013b). *Introductory Lectures on Convex Optimization: A Basic Course*, volume 87. Springer Science & Business Media.

Peng, B. and Wang, L. (2015). An iterative coordinate descent algorithm for high-dimensional nonconvex penalized quantile regression. *Journal of Computational and Graphical Statistics*, 24(3):676–694.

Richtárik, P. and Takač, M. (2014). Iteration complexity of randomized block-coordinate descent methods for minimizing a composite function. *Mathematical Programming*, 144(1):1–38.

Saha, A. and Tewari, A. (2013). On the nonasymptotic convergence of cyclic coordinate descent methods. *SIAM Journal on Optimization*, 23(1):576–601.

Shi, H.-J. M., Tu, S., Xu, Y., and Yin, W. (2016). A primer on coordinate descent algorithms. *arXiv preprint arXiv:1610.00040*.

Smucler, E. and Yohai, V. J. (2017). Robust and sparse estimators for linear regression models. *Computational Statistics & Data Analysis*, 111:116–130.

Sun, Q., Zhou, W.-X., and Fan, J. (2020). Adaptive huber regression. *Journal of the American Statistical Association*, 115(529):254–265.

Sun, Y., Babu, P., and Palomar, D. P. (2016). Majorization-minimization algorithms in signal processing, communications, and machine learning. *IEEE Transactions on Signal Processing*, 65(3):794–816.

Tibshirani, R., Bien, J., Friedman, J., Hastie, T., Simon, N., Taylor, J., and Tibshirani, R. J. (2012). Strong rules for discarding predictors in lasso-type problems. *Journal of the Royal Statistical Society Series B: Statistical Methodology*, 74(2):245–266.

Tseng, P. and Yun, S. (2009). A coordinate gradient descent method for nonsmooth separable minimization. *Mathematical Programming*, 117:387–423.

Wright, S. J. (2015). Coordinate descent algorithms. *Mathematical Programming*, 151(1):3–34.

Wu, T. T. and Lange, K. (2008). Coordinate descent algorithms for lasso penalized regression. *The Annals of Applied Statistics*, pages 224–244.

Yi, C. and Huang, J. (2017). Semismooth Newton coordinate descent algorithm for elastic-net penalized huber loss regression and quantile regression. *Journal of Computational and Graphical Statistics*, 26(3):547–557.

Zou, H. and Hastie, T. (2005). Regularization and variable selection via the elastic net. *Journal of the Royal Statistical Society Series B: Statistical Methodology*, 67(2):301–320.